The effect of non-locality (or size-dependency) on optimum topologies (or material layouts)

M. Tuna[1,2], P. Trovalusci[1] and N. Fantuzzi[2]

**[1]Department of Structural and Geotechnical Engineering,
Sapienza University of Rome, Italy
[2]Department of Civil, Chemical, Environmental, and Materials
Engineering, University of Bologna, Italy**

Abstract

The current work aims to generalize topology optimization problem to scale-dependent two-dimensional plates regarding micropolar and Eringen's theory of elasticity. The material distribution maximizing the structural stiffness are obtained in the framework of solid isotropic material penalization approach, accompanied by density filter and Heaviside projection in order to ensure mesh independent binary solutions. The computational cost is reduced by integrating an element removal and re-introduction strategy. Several benchmark problems are investigated under the assumption of linear elasticity to clearly demonstrate the influence of internal length and different non-locality mechanism on final optimum configurations.

Keywords: non-local, micropolar, Eringen, SIMP, optimization, finite element method

1   Introduction

The mechanical behaviour of materials with comparable internal and external length scales strongly depends on the nature of the underlying structure. To this end, non-classical theories are utilized following their capability of maintaining the information of internal material organization while exploiting the field descriptions [1,2,3,4]. Depending on the nature of non-locality, these theories can be classified as implicit/weak and explicit/strong [4,5,6,7]; in the former class, the body is considered as a collection of particles enriched with additional degrees of freedom (DOFs) resulting in additional field equations, whereas in the latter, the equations of motions

contain different operators while preserving the primal fields of classical theory. Despite their popularity in describing the overall mechanical response of complex structures, till now only limited number of works have targeted their effect on structural optimization problem [8,9,10,11,12,13,14,15,16,17,18].

With this motivation, the present paper generalizes finite element (FE) based topology optimization to the two-dimensional (2D) size-dependent structures in the framework of weakly non-local Cosserat (micropolar) [4] and strongly non-local Eringen's theories [19]. Each element is parametrized by material density that is linked to elasticity modulus following solid isotropic material penalization (SIMP) approach [20]. Numerical issues such as checkerboard pattern and mesh dependency are suppressed by means of density filter [21] while the undesirable transition region (i.e. the *grey zone*), emerged due to filtering is suppressed by means of Heaviside projection method [22]. Lastly, an element removal and reintroduction scheme [23], is embedded to the algorithms to increase computational efficiency and to avoid the misleading contribution of low density elements to structural analysis of Eringen's non-local model. Two example problems of practical importance are studied under the assumption of linear elasticity to compare and discuss the influence of small-scale parameters in different type of non-local theories by focusing on the resulting optimal material layouts.

2   Methods

In micropolar theory, the material particles are described in terms of their positions and rotations, hence the material deformation includes additional micro-rotational degree of freedom, φ, besides displacement, u. The corresponding field equations are given below for a body force and body couple neglected domain.

$$
\begin{aligned}
&\varepsilon_{ij}^{\mathrm{M}} = u_{i,j}^{\mathrm{M}} + e_{ijk}\phi_k, \;\; \chi_{kj} = \phi_{k,j} \\
&\sigma_{ij,j}^{\mathrm{M}} = 0, \; \mu_{kj,j} - e_{ijk}\sigma_{ij}^{\mathrm{M}} = 0 \\
&\sigma_{ij}^{\mathrm{M}}(\mathbf{x}) = \lambda\varepsilon_{kk}^{\mathrm{M}}(\mathbf{x})\delta_{ij} + (\mu+\chi)\varepsilon_{ij}^{\mathrm{M}}(\mathbf{x}) + \mu\varepsilon_{ji}^{\mathrm{M}}(\mathbf{x}), \\
&\mu_{kj}(\mathbf{x}) = \alpha\chi_{ii}(\mathbf{x})\delta_{kj} + \beta\chi_{jk}(\mathbf{x}) + \gamma\chi_{kj}(\mathbf{x})
\end{aligned}
\tag{1}
$$

where $\varepsilon_{ij}^{\mathrm{M}}, \chi_{kj}, \sigma_{ij}^{\mathrm{M}}, \mu_{kj}$ refer to strain, curvature, stress and couple-stress tensors with superscript M denoting micropolar theory. Note that the comma indicates derivation operation. The $\alpha, \beta, \gamma, \chi$ appeared in constitutive equations being material constants related to micropolar theory, while λ, μ stand for generalised Lame's constants:

$$
\lambda = \frac{E\nu}{(1+\nu)(1-2\nu)}, \;\; \mu = G - \frac{\chi}{2}, \;\; G = \frac{E}{2(1+\nu)}
\tag{2}
$$

with E, G, ν being the Young's modulus, shear modulus and Poisson's ratio, respectively. As for Eringen's theory of elasticity, the state of stress at a point; $\mathbf{x}$ is related to strain of all the neighbouring points; $\bar{\mathbf{x}}$ within a certain proximity by means

of an attenuation type kernel function; $\tau(r,\kappa)$ that accounts for the long-range effects between source and neighbouring points depending on their Euclidean distance, r. Ignoring body forces, the field equations are as follows:

$$
\begin{aligned}
&\varepsilon_{ij}^{\mathrm{E}} = \frac{1}{2}\left(u_{i,j}^{\mathrm{E}} + u_{j,i}^{\mathrm{E}}\right) \\
&\sigma_{ij,j}^{\mathrm{E}} = 0 \\
&\sigma_{ij}^{\mathrm{E}}(\mathbf{x}) = \xi t_{ij}^{\mathrm{E}}(\mathbf{x}) + (1-\xi)\int_{\Omega} \tau(r,\kappa) t_{ij}^{\mathrm{E}}(\bar{\mathbf{x}}) d\Omega(\bar{\mathbf{x}}) \\
&t_{ij}^{\mathrm{E}}(\mathbf{x}) = \lambda \varepsilon_{kk}^{\mathrm{E}}(\mathbf{x})\delta_{ij} + 2G\varepsilon_{ij}^{\mathrm{E}}(\mathbf{x})
\end{aligned}
\tag{3}
$$

Independent of the continuum theory to be conducted, the topology optimization problem considered herein aims to find the optimal material distribution that maximizes the stiffness of a structure by minimizing the compliance function under a given set of constraints for a self-weight free domain:

$$
\begin{aligned}
\text{find}: \quad & \boldsymbol{\rho} = \left\{\rho_1, \rho_2, \ldots \rho_{N_{\mathrm{tot}}}\right\} \\
\text{minimize}: \quad & c(\boldsymbol{\rho}) = \mathbf{u}^{\mathrm{T}}\mathbf{f} \\
\text{subj. to}: \quad & \mathbf{r}(\boldsymbol{\rho}) = \mathbf{K}\mathbf{u} - \mathbf{f} = \mathbf{0} \\
& g(\boldsymbol{\rho}) = \frac{V_{\mathrm{tot}}}{V_0} - V_f \leq 0 \\
& 0 \leq \rho_m \leq 1 \quad m = 1,2,\ldots,N_{\mathrm{tot}}
\end{aligned}
\tag{4}
$$

where the displacement vector, $\mathbf{u}$, stiffness matrix, $\mathbf{K}$ and total material volume, V_{tot}, depends on the design variables vector $\boldsymbol{\rho}$ with 0 and 1 referring to void and solid parts, respectively. c stands for the structural compliance function, while $\mathbf{r}$ indicates residual load vector, and g refers to constraint function limiting the material volume to a desired fraction, V_f, with V_0 being the volume of the design domain. To satisfy the volume constraint, the initial density is taken equal to the volume fraction at the beginning of the algorithm; $\rho_{ini} = V_f$. As the direct use of design variables in analysis causes the common issue of checkerboard pattern, and mesh dependence, the formulation needs to be improved through different schemes, such as density filtering. In this case, filtered densities, $\tilde{\boldsymbol{\rho}}$ are obtained by smoothing the original densities with taking into account the status of neighbour elements set, N_m, with the aid of a weighting function, w:

$$
\tilde{\rho}_m(\boldsymbol{\rho}) = \frac{\sum_{q \in N_m} w_{mq}\rho_q}{\sum_{q \in N_m} w_{mq}}, \quad w_{mq} = 1 - \frac{\Delta_{mq}}{r_{\min}} \quad \text{and} \quad q \in N_m \quad \text{if} \quad \Delta_{mq} \leq r_{\min}
\tag{5}
$$

where Δ_{mq} is the center to center distance between elements m and q, while r_{min} refers to user defined filter radius. The drawback of density filter, causing a field with intermediate density values, is diminished by exploiting Heaviside projection method amplifying the continuous filtered field to desired binary solution:

$$\hat{\rho}_m(\boldsymbol{\rho}) = 1 - e^{-\beta\tilde{\rho}_m} + \tilde{\rho}_m e^{-\beta} \tag{6}$$

with β tailoring the curvature of the Heaviside function. It should be noted that to ensure a stable convergence, Heaviside projection method is generally used with a continuation scheme in which β is gradually increased from an initial value, β_{min}, to β_{max}, as the optimization progresses, which are taken as 1 and 36. In this contribution, the problem given in Equation (4) is solved with establishing a gradient-based optimization procedure upon the optimality criteria approach with employing the fixed point iteration method:

$$\rho_m^{t+1} = \rho_m^t \dfrac{-\dfrac{\partial c}{\partial \rho_m}}{\lambda \dfrac{\partial g}{\partial \rho_m}} = \rho_m^t B_m, \quad m = 1, 2, \dots N_{\text{tot}}$$

$$\rho_m^{t+1} = \begin{cases} \max\left(0, \rho_m^t - \overline{\text{m}}\right) & \text{if } \rho_m^t B_m^{\overline{\text{n}}} \leq \max\left(0, \rho_m^t - \overline{\text{m}}\right) \\ \min\left(1, \rho_m^t + \overline{\text{m}}\right) & \text{if } \rho_m^t B_m^{\overline{\text{n}}} \geq \min\left(1, \rho_m^t + \overline{\text{m}}\right) \\ \rho_m^t B_m^{\overline{\text{n}}} & \text{otherwise} \end{cases} \tag{7}$$

where $\overline{n}$ is smoothing factor, and $\overline{m}$ is a positive-move limit which are taken as 0.5 and 0.2, respectively. The sensitivity of compliance can be represented in terms of element stiffness matrices, $\mathbf{k}_0^{\text{M}}$, $\mathbf{k}_0^{\text{E}}$, $\mathbf{k}_{qq0}^{\text{E}}$, $\mathbf{k}_{nq0}^{\text{E}}$ and nodal displacements, $\mathbf{d}_q^{\text{M}}$ $\mathbf{d}_q^{\text{E}}$:

$$\frac{\partial c^{\text{M}}}{\partial \hat{\rho}_q} = -\frac{\partial E_q}{\partial \hat{\rho}_q}\left(\mathbf{d}_q^{\text{M}}\right)^{\text{T}} \mathbf{k}_0^{\text{M}} \mathbf{d}_q^{\text{M}}$$

$$\frac{\partial c^{\text{E}}}{\partial \hat{\rho}_q} = -\frac{\partial E_q}{\partial \hat{\rho}_q}\left(\mathbf{d}_q^{\text{E}}\right)^{\text{T}} \xi_q \mathbf{k}_0^{\text{E}} \mathbf{d}_q^{\text{E}} - \frac{\partial E_q}{\partial \hat{\rho}_q}\left(\mathbf{d}_q^{\text{E}}\right)^{\text{T}}\left(1 - \xi_q\right)\mathbf{k}_{qq0}^{\text{E}} \mathbf{d}_q^{\text{E}} \tag{8}$$

$$- \frac{\partial E_q}{\partial \hat{\rho}_q}\sum_{\substack{n|q \in R_n \\ q \neq n}}\left(\mathbf{d}_n^{\text{E}}\right)^{\text{T}}\left(1 - \xi_n\right)\mathbf{k}_{nq0}^{\text{E}} \mathbf{d}_q^{\text{E}}$$

For explicit expressions of stiffness matrices, the readers refer to [18]. Following the SIMP method, that links physical densities and Young's modulus for which E_{min} and E_0 referring to the modulus of solid and void;

$$E_m(\boldsymbol{\rho}) = E_{\min} + \hat{\rho}_m^p(\boldsymbol{\rho})\left(E_0 - E_{\min}\right) \tag{9}$$

4

the gradient takes the following form:

$$\frac{\partial E_q}{\partial \hat{\rho}_q} = p\left(E_0 - E_{\min}\right)\hat{\rho}_q^{\,p-1} \tag{10}$$

Lastly, it should be mentioned that elements with physical densities below a prescribed threshold, ρ_{tol}, which is taken 0.2 in the current study, carry a negligible contribution to the physical response of the model; hence can be dismissed from the structural analysis, alongside with the nodes completely surrounded by such elements.

3   Results

Two example problems, including plates with and without cracks, are studied to show the effect of each theory on optimum configurations in a comparative manner. To this aim, simply supported intact plate and simply supported plate weakened with two edge cracks of length $0.0625L$ are considered (Figure 1). The latter one is modelled by detaching the nodes placed along the crack lines while for Eringen's model the distorting effect of discontinuity on diffusion process is simply accounted by intercepting the long-range interactions traversing it. Note that the examination of a cracked domain may be regarded as the first step of finding optimal material distribution also in terms of prevention of crack initiation and propagation.
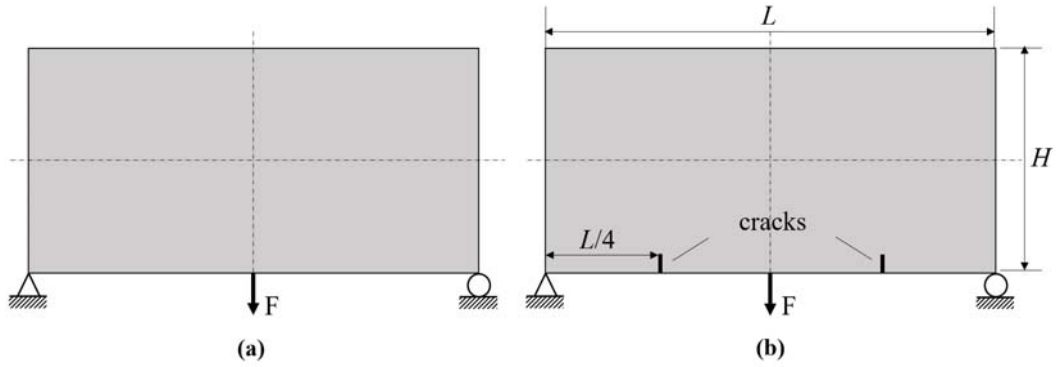
Figure 1: Schematic of comparative examples; (a) intact, (b) weakened plates.

The rectangular design domain, that has an aspect ratio of $L/H=2$, and subjected to a downwards force at the middle of its bottom edge, discretized into 80×40 elements following the mesh independence of the procedure [18]. Numerical problem of hour-glassing is avoided by modelling the concentrated load as a distributed one with a very small span; $L/20$, while optimization process is performed for the following parameter set:

$$E = 1.0,\, v = 0.3,\, V_f = 0.5,\, \beta_{ini} = 0,\, \beta_{\max} = 36,\, r_{\min} = 0.0375L,\, \rho_{tol} = 0.20 \tag{11}$$

where various internal lengths are considered to observe the effect of non-locality:

$$\text{Micropolar}: \quad N = 0.75, \ l_c \,/\, L = 0.0125 - 0.0375$$
$$\text{Eringen}: \qquad \xi = 0.25, \ \kappa \,/\, L = 0.0125 - 0.0375 \tag{12}$$

Here the largest value of characteristic internal length is limited to $0.0375L$ to avoid the need of incorporation of *geodetic path* in Eringen's model while the coupling number, N, and the fraction coefficient, ξ, are kept fixed at 0.75 and 0.25, for which the material response is more sensitive to corresponding internal length scale of the continua.

$N= 0.75, l_c = 0.0375L$

$c = 9.42$ $c = 9.55$

$N= 0.75, l_c = 0.0250L$

$c = 10.12$ $c = 10.26$

$N= 0.75, l_c = 0.0125L$

$c = 10.63$ $c = 11.03$

(a) **(b)**
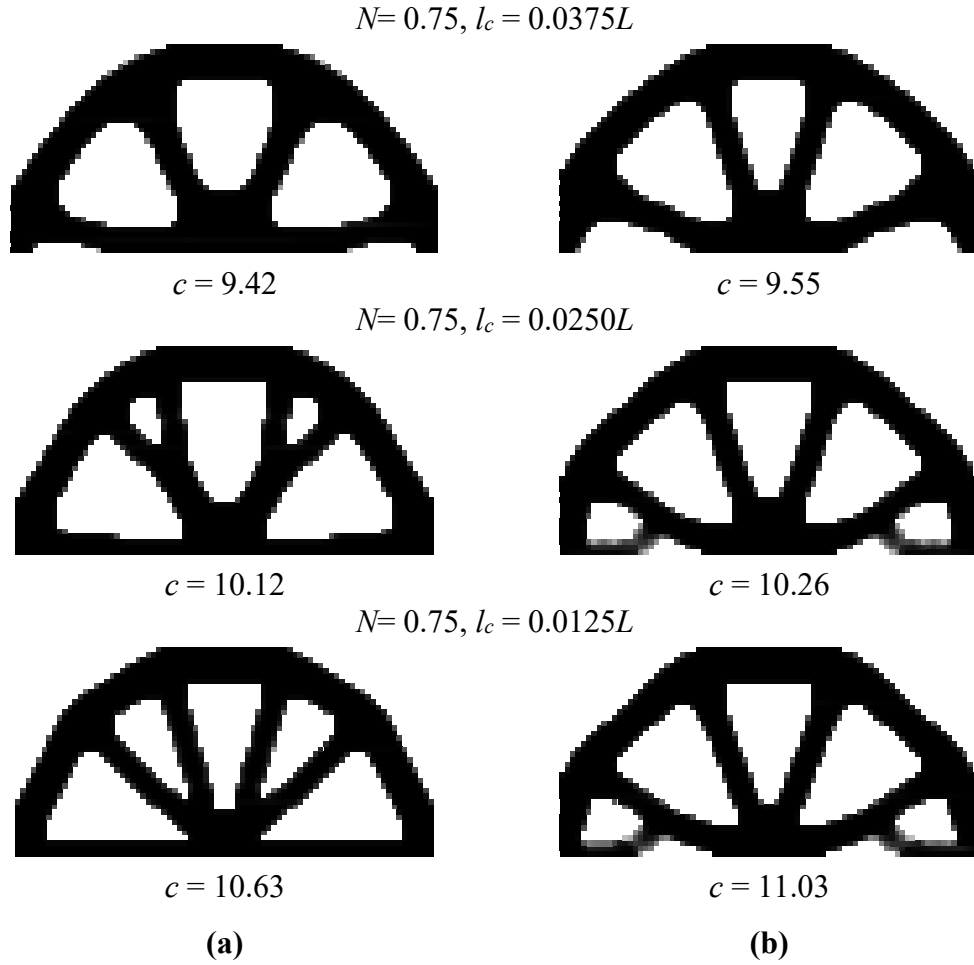
Figure 2: Optimum material distributions and corresponding compliances for different material properties of micropolar continuum considering comparative (a) intact and (b) weakened plates.

From the evolution of the optimum topologies, illustrated in Figures 2 and 3, following deductions can be made. In micropolar medium (Figure 2), the scale effect unites the internal braces and thickens the junctions of them to the main arch, providing curved members instead of straight ones since the couple-stress tensor is highly affected by the parameter l_c, given the high value of coupling number and dominant bending effects in the problem. It is easy to observe that there is no material

formation around the crack region in order to avoid stress singularity. Moreover, additional branches on the bottom corners for l_c=0.0125L and l_c=0.0250L are lost in case of l_c=0.0375L, and replaced with thicker connections to the main arch due to increased capacity of rotation resistance of the material points. As for strong non-local model, although no significant variation from Cauchy medium is present, as depicted in Figure 3, internal braces are slightly narrowed down. Similar comments apply to the case of cracked region. An increase in grey zones are observed for increasing non-locality; however, note that use of *geodetic path* may have an effect on the final topology in this case.

$\xi = 0.25, \kappa = 0.0375L$

| $c = 17.72$ | $c = 18.16$ |

$\xi = 0.25, \kappa = 0.0250L$

| $c = 16.02$ | $c = 16.54$ |

$\xi = 0.25, \kappa = 0.0125L$

| $c = 13.68$ | $c = 14.20$ |

(a)   **(b)**
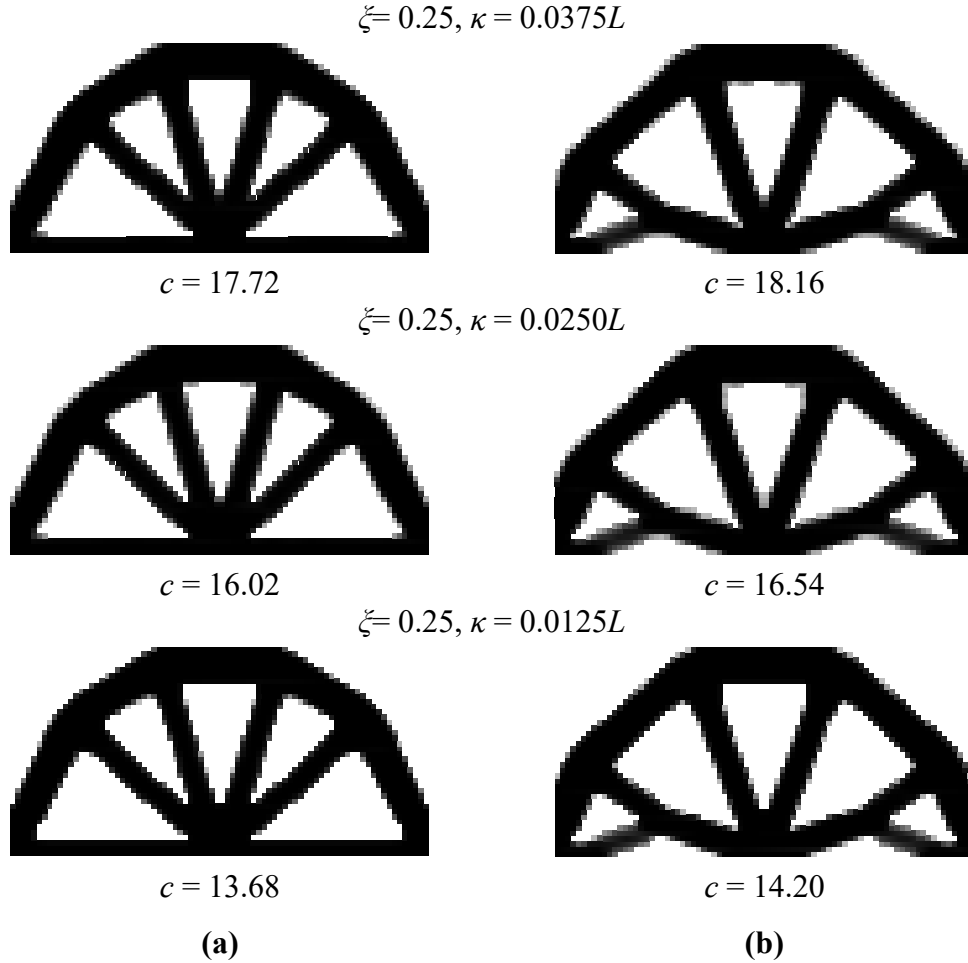
Figure 3: Optimum material distributions and corresponding compliances for different material properties of Eringen continuum considering comparative (a) intact and (b) weakened plates.

Finally, Figure 4 shows the contribution of the elements to the compliance in the optimized configurations for all the examples. These contributions are evaluated by calculating the strain energy of each element individually, and weighted with the total value of compliance in order to compare different theories. The extreme values at the loading and boundary regions are off the scale for all sub-figures, for the sake of seeing better the distribution. The Cosserat continuum seems to be the one with the

least strain energy gradient, which is pointing out its ability to distribute the load. It has the lowest compliance among all continua descriptors for both example problems. Although the final topologies of Eringen continuum are quite similar to that of Cauchy, the contribution of the internal braces to the compliance is lower than that of the main arms, on the contrary to Cauchy continuum. Moreover, the localized decrement of the stiffness around the boundaries due to missing neighbour relations in Eringen's theory has a negative impact on overall stiffness distribution, leading to the highest compliance values for all problems among the different continua considered herein. Lastly, İn all cases, the macro-scale optimum topologies are in accordance with the laws defining the interactions between material points in micro/nano/scale.

4   Conclusions and Contributions
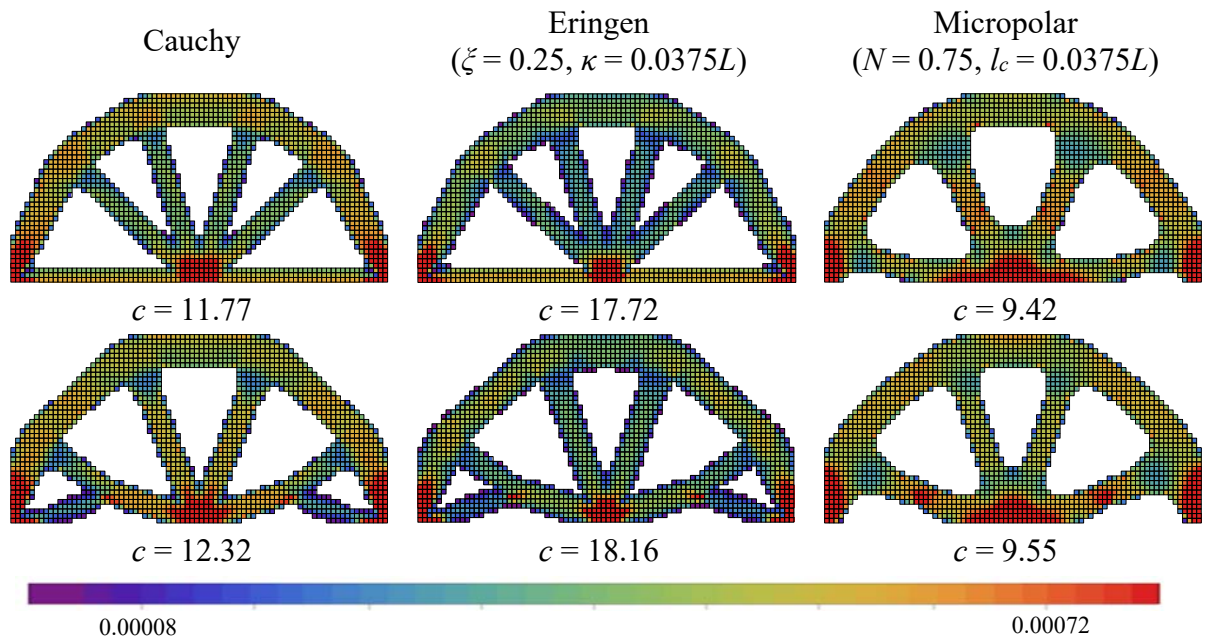
Figure 4: Contribution of the elements to the compliance for different continua descriptors for intact (first row) and weakened (second row) plates

Generalizing topology optimization method to non-classical continuum theories has the ultimate significance in maximizing the performance of size-dependent structures. To this aim, the formulation of standard FE-based optimization problem is extended to analyze the optimal material distributions in domains described on the basis of micropolar and Eringen's theories as representatives of weak and strong non-local models, respectively. Based on the results, following interpretations can be made regarding the effect different non-locality mechanisms with different intensities:
-    The increased capacity of rotation resistance in micropolar case allows a dramatic reduction of structural compliance with the least gradient.

- The topology of Eringen's medium is mainly formed by the localized decrement of the stiffness that occurs around domain boundaries due to missing long-range interactions.
- The macro-scale optimum topologies admit the physics of underlying lattice system with being in accordance with the response governed by particle interactions.

Acknowledgements

References

[1]   R.D. Mindlin, "Micro-structure in linear elasticity", Arch. Ration Mech. Anal. 16, 51–78, 1964.

[2]   I.A. Kunin, "The theory of elastic media with microstructure and the theory of dislocations", in "Mechanics of Generalized Continua", E. Kröner (Editor), Springer, Berlin Heidelberg, 321–329, 1968.

[3]   G. Capriz, "Continua with microstructure", Springer Tracts in Natural Philosophy, Springer-Verlag, 1989.

[4]   A. Eringen, "Microcontinuum Field Theory", Springer, 1999.

[5]   I. Kunin, "On foundations of the theory of elastic media with microstructure", Int. J. Eng. Sci., 22, 969–978, 1984.

[6]   G. Maugin, "Material inhomogeneities in elasticity", Applied Mathematics, Taylor & Francis, 1993.

[7]   P. Trovalusci, "Molecular approaches for multifield continua: origins and current developments", in T. Sadowski, P. Trovalusci (Editors), "Multiscale Modeling of Complex Materials: Phenomenological, Theoretical and Computational Aspects", Springer, Vienna, 211–278, 2014.

[8]   M. Rovati, D. Veber, "Optimal topologies for micropolar solids", Struct Multidisc Optim, 33, 47–59, 2007.

[9]   S. Liu, W. Su, "Topology optimization of couple-stress material structures", Struct Multidisc Optim, 40, 319–326, 2009.

[10]   Y. Arimitsu, K. Karasu, Z. Wu, Y. Sogabe, "Optimal topologies in structural design of micropolar materials", Procedia Eng., 10, 1633–1638, 2011.

[11]   D. Veber, A. Taliercio, "Topology optimization of three-dimensional non-centrosymmetric micropolar bodies", Struct Multidisc. Optim., 45, 575–587, 2012.

[12]   M. Bruggi, A. Taliercio, "Maximization of the fundamental eigen frequency of micropolar solids through topology optimization", Struct Multidisc Optim 46, 549–560, 2012.

[13] L. Li, K. Khandelwal, "Topology optimization of structures with length-scale effects using elasticity with microstructure theory", Comput Struct, 157, 165–177, 2015.

[14] L. Li, G. Zhang, K. Khandelwal, "Topology optimization of structures with gradient elastic material", Struct Multidisc Optim., 56, 371–390, 2017.

[15] D. Da, J. Yvonnet, L. Xia, M.V. Le, G. Li, "Topology optimization of periodic lattice structures taking into account strain gradient", Comput Struct, 210, 28–40, 2018.

[16] W. Su, S. Liu S, "Size-dependent microstructure design for maximal fundamental frequencies of structures", Struct Multidisc Optim. 62, 543–557, 2020.

[17] L. Chen, J. Wan, X. Chu, H. Liu, "Parameterized level set method for structural topology optimization based on the Cosserat elasticity", Acta Mech Sin., 37, 620–630, 2021.

[18] M. Tuna, P. Trovalusci, "Topology optimization of scale-dependent non-local plates", Struct Multidisc Optim. 65, 248, 2022.

[19] A. Eringen, "Nonlocal Continuum Field Theories", Springer-Verlag, 2002.

[20] M. Bendsøe, "Optimization of structural topology, shape, and material", Springer, Berlin, 1995.

[21] B. Bourdin, "Filters in topology optimization", Int J Numer Methods Eng, 50, 2143–2158, 2001.

[22] J.K. Guest, J.H. Prevost, T. Belytschko, "Achieving minimum length scale in topology optimization using nodal design variables and projection functions", Int J Numer Methods Eng, 61, 238–254, 2004.

[23] T.E. Bruns, D.A. Tortorelli, "An element removal and reintroduction strategy for the topology optimization of structures and compliant mechanisms", Int J Numer Methods Eng, 57,1413–1430, 2003.